Bone 49 (2011) 395–403

Contents lists available at ScienceDirect

Bone

journal homepage: www.elsevier.com/locate/bone

Absence of the lysophosphatidic acid receptor LPA1 results in abnormal bone development and decreased bone mass☆,☆☆

Isabelle Gennero [a,b,*,1], Sara Laurencin-Dalicieux [a,d,1], Françoise Conte-Auriol [a,c], Fabienne Briand-Mésange [a], Danielle Laurencin [e], Jackie Rue [d], Nicolas Beton [a], Nicole Malet [a], Marianne Mus [a,c], Akira Tokumura [f], Philippe Bourin [g], Laurence Vico [h,k], Gérard Brunel [d], Richard O.C. Oreffo [i], Jerold Chun [j], Jean Pierre Salles [a,c,*]

[a] INSERM Unité 1043 (Centre de Physiopathologie de Toulouse Purpan), Université Paul-Sabatier, Hôpital Purpan, CHU de Toulouse, 31059 Toulouse Cedex 9, France
[b] Institut Fédératif de Biologie, Laboratoire de Biochimie, CHU de Toulouse, 31059 Toulouse Cedex 9, France
[c] Endocrine and Bone Diseases Unit, Hôpital des Enfants, CHU de Toulouse, 31059 Toulouse Cedex 9, France
[d] Faculté de Chirurgie Dentaire, Université Paul-Sabatier, 3 Chemin des Maraîchers, 31062 Toulouse Cedex, France
[e] Institut Charles Gerhardt de Montpellier, UMR 5253, CNRS-UM2-ENSCM-UM1, Université Montpellier 2, CC1701, Place Eugène Bataillon, 34095 Montpellier Cedex 5, France
[f] Department of Health Chemistry, Institute of Health Biosciences, University of Tokushima Graduate School, 1-78-1 Shomachi, Tokushima, Japan
[g] Etablissement Français du Sang Pyrénées-Méditerranée, 75 Rue de Lisieux, 31300 Toulouse, France
[h] Université de Lyon, F42023 Saint-Etienne, France
[i] Bone and Joint Research Group, Centre for Human Development, Stem Cells and Regeneration, Institute of Developmental Sciences, University of Southampton Medical School, Southampton SO16 6YD, UK
[j] Department of Molecular Biology, Dorris Neuroscience Center, The Scripps Research Institute, 10550 N. Torrey Pines Rd., ICND-118, La Jolla, CA, USA
[k] INSERM U890/IFR143, F-42023 Saint-Etienne, France

ARTICLE INFO

Article history:
Received 31 December 2010
Revised 7 April 2011
Accepted 20 April 2011
Available online 1 May 2011

Edited by: Bjorn Olsen

Keywords:
Lysophosphatidic acid
LPA_1
Bone
Osteoblast
Mesenchymal stem cell
Osteogenesis

ABSTRACT

Lysophosphatidic acid (LPA) is a lipid mediator that acts in paracrine systems via interaction with a subset of G protein-coupled receptors (GPCRs). LPA promotes cell growth and differentiation, and has been shown to be implicated in a variety of developmental and pathophysiological processes. At least 6 LPA GPCRs have been identified to date: LPA_1–LPA_6. Several studies have suggested that local production of LPA by tissues and cells contributes to paracrine regulation, and a complex interplay between LPA and its receptors, LPA_1 and LPA_4, is believed to be involved in the regulation of bone cell activity. In particular, LPA_1 may activate both osteoblasts and osteoclasts. However, its role has not as yet been examined with regard to the overall status of bone *in vivo*. We attempted to clarify this role by defining the bone phenotype of $LPA_1^{(-/-)}$ mice. These mice demonstrated significant bone defects and low bone mass, indicating that LPA_1 plays an important role in osteogenesis. The $LPA_1^{(-/-)}$ mice also presented growth and sternal and costal abnormalities, which highlights the specific roles of LPA_1 during bone development. Microcomputed tomography and histological analysis demonstrated osteoporosis in the trabecular and cortical bone of $LPA_1^{(-/-)}$ mice. Finally, bone marrow mesenchymal progenitors from these mice displayed decreased osteoblastic differentiation. These results suggest that LPA_1 strongly influences bone development both qualitatively and quantitatively and that, *in vivo*, its absence results in decreased osteogenesis with no clear modification of osteoclasis. They open perspectives for a better understanding of the role of the LPA/LPA_1 paracrine pathway in bone pathophysiology.

☆ Funding sources: This work was supported by grants from the French Program of Hospital Clinical Research (PHRC, AOL 0304602), from the Conseil Régional de Midi-Pyrénées (Cellular and Gene Therapy Program) and from the Etablissement Français du Sang (EFS) (Program 2003.02). J. Chun was supported by grants from the NIH: MH051699 and NS048478. S. Laurencin-Dalicieux is the recipient of a grant provided by Pfizer France. R. Oreffo is supported by the Biotechnology and Biological Sciences Research Council. J.P. Salles was supported by a grant provided by Pfizer France (convention 08766A10).

☆☆ Conflict of interest. All authors have no conflict of interest.

* Corresponding authors at: INSERM Unité 1043 (Centre de Physiopathologie de Toulouse Purpan), Bâtiment C, Hôpital Purpan, 31059 Toulouse Cedex 9, France. Fax: +33 5 62 74 86 50.

E-mail addresses: gennero.i@chu-toulouse.fr (I. Gennero), sara.laurencin@inserm.fr (S. Laurencin-Dalicieux), crc@chu-toulouse.fr (F. Conte-Auriol), fabienne.briand-mesange@inserm.fr (F. Briand-Mésange), danielle.laurencin@univ-montp2.fr (D. Laurencin), rue@cict.fr (J. Rue), nicolas.beton@inserm.fr (N. Beton), nicole.malet@inserm.fr (N. Malet), marianne.mus@inserm.fr (M. Mus), tokomura@ph.tokushima-u.ac.jp (A. Tokumura), philippe.bourin@efs.sante.fr (P. Bourin), vico@univ-st-etienne.fr (L. Vico), brunel@cict.fr (G. Brunel), roco@soton.ac.uk (R.O.C. Oreffo), jchun@scripps.edu (J. Chun), salles.jp@chu-toulouse.fr (J.P. Salles).

[1] These authors contributed equally to the work.

8756-3282/$ – see front matter © 2011 Elsevier Inc. All rights reserved.
doi:10.1016/j.bone.2011.04.018

Introduction

The identification of the mechanisms that promote skeletal growth and bone formation has significant implications in pathophysiology and medicine. Building up adequate bone mass, potentially influenced by genetic factors during development, is essential for a healthy skeleton and subsequent minimal fracture incidence throughout life [1]. With the help of animal models, there is increasing evidence that local molecular factors strongly influence the building up of bone mass through induction and regulation of osteoblast proliferation and differentiation. Lysophosphatidic acid (LPA) is a potent lipid mediator that acts in paracrine systems via interaction with a subset of G protein-coupled receptors (GPCRs). Based on the recently revised international nomenclature, 6 GPCRs have been identified to date for LPA, LPA_1–LPA_6 [2]. LPA may be present in the systemic circulation in micromolar concentrations, numerous studies having demonstrated that the local production of LPA by tissues and cells highly contributes to paracrine regulation [3–5]. LPA promotes cell growth, motility and differentiation, and has been shown to be implicated in a variety of developmental and pathophysiological processes [6–8]. An increasing interest is attached to the possibility of targeting LPA or LPA receptors for medical purposes [9].

A complex interplay between LPA and its receptors is believed to be involved in the regulation of osteoblast differentiation and bone formation. Thus, LPA induces proliferation of osteoblasts through a pathway that involves G_i proteins and cytosolic calcium [10–12] as well as osteoclast activation [13]. Lysophosphatidic acid synergistically co-operates with calcitriol to promote maturation of the human osteosarcoma cell line, MG63 [14]. In addition, this study demonstrated the dependence on G_i to differentiate mature osteoblasts under LPA. Such an effect of LPA on mature osteoblasts is in agreement with its described role in promoting dendrite outgrowth of the osteocyte-like cell line, MLO-Y4 [15,16]. LPA induces changes in the cytoskeleton and stimulates the migration of MC3T3-E1 osteoblastic cells [17]. It has also been shown to induce membrane blebbing in mouse primary osteoblasts [18]. Moreover, activation of the P2X7 receptor leads to LPA production and increases mineralization [19].

As recently demonstrated, LPA_4 inhibits osteoblastic differentiation of stem cells and LPA_4-deficient mice have increased bone mass [20]. LPA_1 knock-out mice ($LPA_1^{(-/-)}$) exhibit impaired suckling behavior and neurological abnormalities [21]. Nevertheless, the role of the LPA_1 receptor has to this day not been extensively examined with regard to the *in vivo* bone status.

A key point is that, given the complex actions of LPA_1 on osteogenesis as well as osteoclasis, and the negative role played by LPA_4 on bone mass, the real role of LPA_1 remains elusive. We have attempted to clarify the role of the LPA_1 receptor by defining the bone phenotype of $LPA_1^{(-/-)}$ mice. This study is to our knowledge the first to document the potential role of LPA_1 *in vivo* in bone mass and bone development. These mice were studied by microcomputed tomography (μCT) and histological analysis. Finally, bone marrow mesenchymal progenitors from $LPA_1^{(-/-)}$ mice were tested for proliferation rate and osteoblastic differentiation. The overall results clearly suggest a positive role of LPA_1 in bone development and bone formation, with $LPA_1^{(-/-)}$ mice presenting decreased bone mass and specific skeletal abnormalities. This may open future perspectives targeting LPA receptors for the control of bone mass.

Materials and methods

Animals and reagents

For this study, the $LPA_1^{(-/-)}$ mice initially generated by Contos et al. [21] were transferred and maintained in a C57BL/6 background. All data in this study are derived from this strain. Mice were genotyped using PCR analysis of tail or ear DNA to identify homozygous WT (wild-type) or $LPA_1^{(-/-)}$ mice as previously described [21]. All experiments were performed in accordance with the principles and guidelines established by the French Institute of Medical Research, INSERM, employing the principles and procedures dictated by the highest standards of humane animal care. Growth evaluation was also performed with the initial 129SvJ/C57BL6 and newly generated knock-out mouse strain. Body length (crown-rump distance) was measured at 1, 2 and 4 weeks of age, and femur and tibia lengths were measured at 2 and 4 weeks.

All reagents were purchased from Sigma-Aldrich (St. Louis, MO, USA), unless otherwise indicated.

Whole mount alizarin red and alcian blue staining

Whole mount skeletal staining was conducted as described previously, with slight modifications [22]. Briefly, mice were anesthetized, eviscerated, skinned, and stained in alcian blue (AB) solution (0.02% AB (w/v), 70% ethanol (v/v), 30% acetic acid (v/v)) for 1 to 2 days at room temperature. Samples were washed through a descending ethanol series, i.e.: 100%, 100%, 95%, 70%, 40%, and 15% ethanol/distilled water (v/v), 1 h each, rinsed twice in distilled water and immerged in distilled water for 1 h. Sample were then treated with 1% (w/v) trypsin, 1 g trypsin digesting 250 g of casein substrate (Invitrogen Molecular Probes, Carlsbad, CA, USA) in 140 mM NaCl solution for 4 h. After rinsing with 140 mM NaCl solution, samples were transferred in 1% (w/v) KOH solution containing 0.1% (w/v) alizarin red S (AR) dye for 24 h at room temperature. Finally, samples were washed through a graded series of 1% (w/v) KOH/glycerol 3/1, 1/1, and 1/3 (v/v), 24 h each, visualized and stored in 100% (v/v) glycerol.

Radiological and histological analysis

Plain radiographs were taken using a soft X-ray apparatus (Softex CMB-2, Softex, Kanagawa, Japan). For histological analysis, some skeletons were fixed in 70° ethanol/distilled water (v/v), embedded in metacrylate and stained with alizarin red according to standard procedures.

High-resolution microcomputed tomography

Femurs and vertebrae of 4-week-old mice were scanned with a high resolution μCT prototype (VivaCT40, Scanco Medical AG, Brüttisellen, Switzerland) as described by Kohlbrenner et al. [23]. At a 3D level, the following calculations were made as previously published [24]: relative bone volume over total bone volume (BV/TV), bone surface over bone volume (BS/BV), trabecular number (Tb.N), trabecular thickness (Tb.Th), trabecular separation (Tb.Sp), and bone mineral density (BMD_{trab}). Connectivity density (Conn.D) and structure model index (SMI) were calculated without assuming a constant model, as previously described [24]. SMI estimates the plate–rod characteristics of a structure; its value is 0 for an ideal plate and 3 for an ideal rod, with intermediate values reflecting the volume ratio between rods and plates. The geometric degree of anisotropy (DA) is defined as the ratio between the maximal and minimal radius of the mean intercept length (MIL) ellipsoid. DA reduction is correlated with a more isotropic bone structure.

To analyze the femoral cortex, cross-sectional slices were chosen and the following parameters were calculated: cortical thickness (Ct.Th), cortical area (Ct.Ar), marrow area (Ma.Ar), cross-sectional total area (T.Ar), and cortical bone mineral density (BMD_{cort}).

Cell cultures

mBMSC (murine bone marrow stromal cells) were obtained from the bone marrow of femurs and tibias of WT and $LPA_1^{(-/-)}$ mice essentially as described elsewhere [25]. Cells were maintained in modified Eagle medium alpha (αMEM) with 10% (v/v) fetal calf serum

(FCS) before use. For proliferation assay, cells were seeded at 20 000 cells per well in 12-well plates and cultured for up to 10 days in a medium consisting of αMEM supplemented with 10% (v/v) FCS. The cells were harvested 2 days after seeding (D0), and later at D3, D7 and D10. For mineralization assays, cells were cultured for up to 14 days in DMEM with 10% FCS (v/v), 100 μM L-ascorbate 2-phosphate as an osteogenic medium (OM) with 10 mM inorganic phosphate essentially as described elsewhere [25].

DNA assay

Cell layers were washed in PBS, scraped with 0.1% (v/v) NP40 and sonicated. The DNA content was measured using the Picogreen® assay according to the manufacturer's instructions (Invitrogen Molecular Probes, Carlsbad, CA, USA).

Mineralization assay

Calcium deposits from WT and LPA$_1^{(-/-)}$ cultured cells were stained with 40 mM AR solution, pH = 4.2, as described previously [26]. Briefly, at days 7 and 14 the medium was removed and wells rinsed twice with phosphate buffer saline (PBS). Cells were fixed in 70% ethanol/distilled water (v/v) for 1 h at 4 °C. AR solution was added to each well for 5 min and rinsed 7 times in order to remove non-specific staining.

Detection of serum biological markers

In order to evaluate their nutritional and mineral status, WT and LPA$_1^{(-/-)}$ mice were bled by retro-orbital puncture at 4 weeks. Blood samples were allowed to clot for 30 min and centrifuged for 10 min at 3000 rpm. Levels of serum glucose, iron, albumin, vitamin D, calcium, magnesium, total proteins, phosphorus and CTX-I were measured using conventional enzymatic methods with an Olympus AU400 biochemistry auto-analyzer.

Real time RT-PCR

After removing the bone marrow and grinding the bones, total RNA from WT and LPA$_1^{(-/-)}$ radius and humerus was isolated using Trisol solution and quantified using an Agilent Ribogreen assay (Invitrogen Molecular Probes, Carlsbad, CA, USA) as described [27]. RNA was reverse transcribed to cDNA using the SuperArray RT2 First Strand kit (Tebu-bio Laboratories, Le Perray en Yvelines, France) according to the manufacturer's instructions. Amplification of the cDNA and detection of the target PCR product were conducted in an ABI Prism 7000 sequence detection system (Applied Biosystems, Carlsbad, CA, USA), using the SuperArray Custom RT2 Profiler PCR Array (Tebu-bio Laboratories, Le Perray en Yvelines, France) according to the manufacturer's instructions. The targets measured included: Col 1, osteocalcin (OC), osterix (OSX), PTHR1 (parathyroid hormone receptor 1), dentin mineral protein 1 (DMP1) and alkaline phosphatase (ALP). RANK (receptor activator of nuclear factor κB), RANKL (RANK ligand), osteoprotegerin (OPG), LPA_2, LPA_3, LPA_4 and autotaxin (ATX) primers were purchased from SABiosciences (Frederick, MD, USA). In order to detect LPA_1 expression, forward 5′-ACTGTTAGCACGTGGCTCCT and reverse 3′-GTTGAAAATGGCCCAGAAGA primers were designed with the Primer3 software tool (Biomatters Ltd, Auckland, New Zealand). The RT-PCR results were analyzed using sequence detection software from Applied Biosystems (Carlsbad, CA, USA), and the relative amount of target gene transcript was normalized to the amount of HPRT mRNA control transcript. The data represent results of RNA analyses from 4 different independent experiments obtained with 10 WT and LPA$_1^{(-/-)}$ mice. The data shown represent the relative mRNA levels calculated as $2-\Delta Ct\times 106$ where $\Delta Ct = Ctgene\ of\ interest - CtHsp90$.

Quantification of LPA

After 12 h of fasting, 4-week-old WT and LPA$_1^{(-/-)}$ mice were bled by retro-orbital puncture and the citrated plasma was carefully centrifuged in order to prevent platelet activation and clotting. LPA was butanol-extracted from mouse plasma or bone marrow and quantified using a radioenzymatic assay as described previously [28]. In short, in the presence of [^{14}C] oleoyl-CoA, recombinant rat LPA acyl-transferase selectively catalyzes the transformation of LPA into [^{14}C] phosphatidic acid. Products of the reaction were separated by one-dimensional thin-layer chromatography and autoradiographed. In these conditions, minimal detection of LPA was 0.2 pmol.

Infrared spectroscopy

Infrared spectra were recorded from KBr pellets on a Nicolet Thermo Avatar 320 FTIR spectrometer between 400 and 4000 cm^{-1}. After removing the bone marrow, each sample of tibia and femur cortical bone tissue was ground into 100 mg of IR-grade KBr prior to pelletization. For each spectrum, intensities of the bands between 1670 and 1500 cm^{-1} (which represent vibrations of the collagenous matrix) were compared to those at 1034, 607, and 572 cm^{-1} (corresponding to the phosphate vibrations of the apatite phase) in order to determine the degree of mineralization of the bone tissue [29,30].

Statistical analysis

Results are expressed as means ± (SD). Groups were compared using Mann–Whitney analyses as appropriate. A p value <0.05 was considered statistically significant.

Results

Skeletal development is altered in LPA$_1^{(-/-)}$ mice

Skeletal preparations of 4-week-old mice stained with alcian blue and alizarin red showed homogeneous dwarfism in LPA$_1^{(-/-)}$ mice, as previously described [21] (Fig. 1A). LPA$_1^{(-/-)}$ mice also displayed previously described cranial deformities including shorter snouts and more widely spaced eyes compared with control siblings. Strikingly, 100% of the LPA$_1^{(-/-)}$ mice analyzed also displayed rib cage deformity. All mice presented several sterno-distal rib fusions (Fig. 1A, close-up). However, the abnormal patterning was not specific to a single pair of ribs and sometimes affected two consecutive costal elements. In addition, the sternebrae, or segments of the sternum, of LPA$_1^{(-/-)}$ mice were shorter, crooked and thicker. Some were even triangular, and the number (normally 7) was typically reduced to 6. The sternum thus appeared sinusoidal (Fig. 1A, close-up), suggesting that the LPA_1 receptor plays a role in the development of sternal cartilage and bone. However, the 1st and 2nd sterno-distal ribs were unaffected. The number and shape of ribs were normal in the proximal and vertebro-distal parts of the dorsal segment. Taken together, these observations suggest that the ventral mesenchymal and costo-vertebral connections are altered due to the absence of LPA_1. Dorsal ossification of the ribs does not appear to be affected.

Most interestingly, we observed delayed vertebral calcification and closure in the thoracic spine of LPA$_1^{(-/-)}$ mice at 2 weeks of age (Fig. 1B, arrow). Complete ossification was however achieved 2 weeks later. All vertebral extremities remained thicker in the 4-week-old LPA$_1^{(-/-)}$ mice (blue stain, Fig. 1A, arrow), also indicating growth plate immaturity.

Thus, the overall phenotype of LPA$_1^{(-/-)}$ mice indicates that LPA_1 plays a role in the processes of skeletal development, especially those involving sternocostal and vertebral elements.

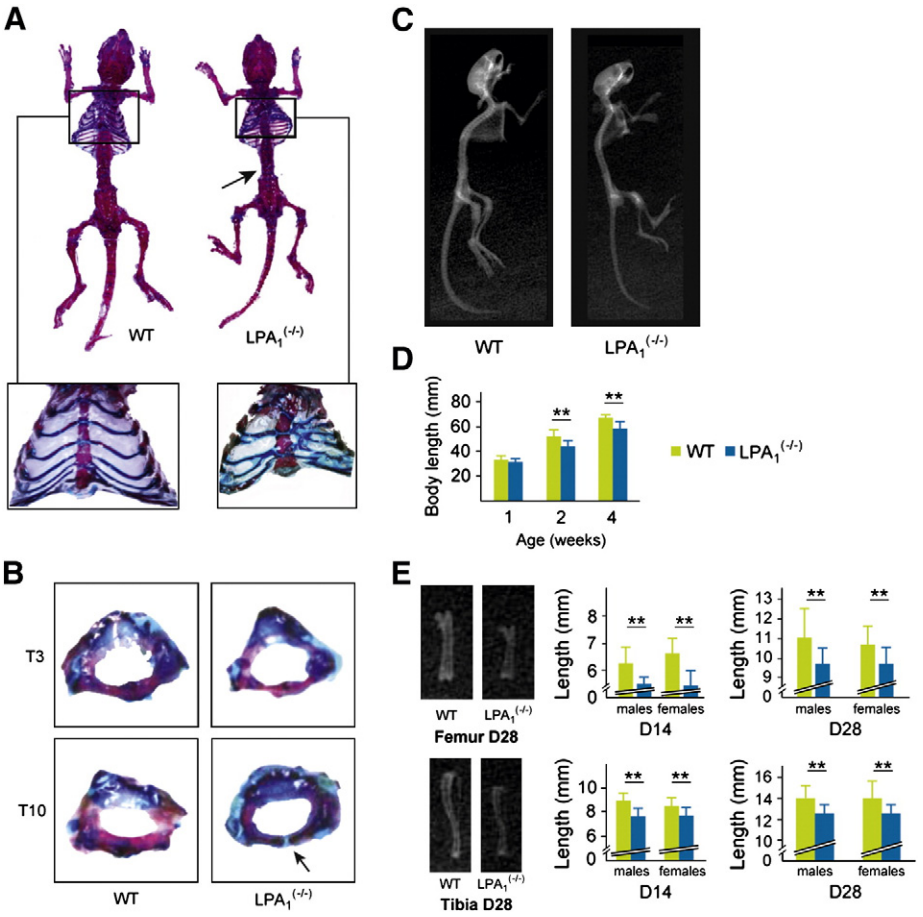

Fig. 1. Gross phenotype of LPA$_1^{(-/-)}$ mice.Alizarin red S (AR) and alcian blue (AB) staining and X-ray analysis of LPA$_1^{(-/-)}$ and WT littermates. (A) Skeletal staining of 4-week-old LPA$_1^{(-/-)}$ and WT mice showing homogeneous dwarfism in LPA$_1^{(-/-)}$ mice (n = 10). These mice also show increased AB staining suggesting an alteration in the bone mineralization process. Close-up AR/AB staining of LPA$_1^{(-/-)}$ and WT mice rib cages demonstrates multiple sterno-distal rib fusions and sternebrae abnormalities. Arrow: AB staining of intervertebral discs and vertebral extremities. (B) At D14, LPA$_1^{(-/-)}$ thoracic vertebrae are smaller and not fully mineralized (arrow) when compared with WT littermates. (C) Profile whole-body X-ray analysis of the skeleton of 4-week-old LPA$_1^{(-/-)}$ and WT mice showing homogeneous dwarfism and less mineralization in LPA$_1^{(-/-)}$ vertebrae and long bones. (D) Growth curves of 1-, 2-, and 4-week-old LPA$_1^{(-/-)}$ mice (black columns) and WT mice (white columns) (n = 10, 15 and 10, respectively). (E) Representative X-ray analysis of 4-week-old LPA$_1^{(-/-)}$ and WT mice femurs (upper left) and tibias (lower left) showing size and mineralization differences. Femur lengths of 2- and 4-week-old male and female LPA$_1^{(-/-)}$ mice (blue columns) and WT mice (green columns) (n = 6) (upper middle and right). Tibia lengths of 2- and 4-week-old male and female LPA$_1^{(-/-)}$ mice (black columns) and WT mice (white columns) (n = 6) (lower middle and right). LPA$_1^{(-/-)}$ femurs and tibias are smaller and less mineralized in the cortical and trabecular areas of the bone than WT littermates.Values are means (SD). Significant statistical differences between groups: **p<0.01, LPA$_1^{(-/-)}$ *vs.* WT by the Mann–Whitney test.

LPA$_1^{(-/-)}$ mice exhibit abnormal growth

LPA$_1^{(-/-)}$ mice were described as having short snouts and small heads in the original study [21]. Radiographic analysis of 4-week-old LPA$_1^{(-/-)}$ mice confirmed this craniofacial phenotype (Fig. 1C). In addition, the short stature of LPA$_1^{(-/-)}$ mice was due to growth defects in the limbs as well as the vertebrae (Figs. 1C–E). Growth retardation was moderate at 1 week of age, the pups having a crown-rump length approximately 95% that of WT pups (31.6 (±3.63) *vs.* 33.2 (±5.63) mm, respectively) (Fig. 1D). Dwarfism became more apparent as the LPA$_1^{(-/-)}$ mice grew. The difference in crown-rump lengths between LPA$_1^{(-/-)}$ mice and their WT littermates reached 15.7% at 2 weeks after birth (44.6 (±4.45) *vs.* 52.9 (±6.12), $p<0.001$), and 13.1% at 4 weeks (58.8 (±12.4) *vs.* 67.7 (±5.06), $p<0.004$) (Fig. 1D). Anthropometric analysis using soft X-rays showed decreased length of a number of skeletal components, particularly limb bones, in LPA$_1^{(-/-)}$ mice (Fig. 1E). The femoral and tibial longitudinal lengths were decreased by 20% (6.55 mm (±0.46) *vs.* 5.47 (±0.36), $p<0.001$) and by 16% (8.85 mm (±0.59) *vs.* 7.65 (±0.52), $p<0.001$), respectively, in 2-week-old LPA$_1^{(-/-)}$ mice (Fig. 1E). The difference remained significant at 4 weeks of age (Fig. 1E). No differences in lengths were observed between males and females at any stage. Lower mineral content was also apparent in the femur and tibia of LPA$_1^{(-/-)}$ mice at 4 weeks, especially in cortical bone (Figs. 1E, left). The profile X-ray analysis of the LPA$_1^{(-/-)}$ mice suggested decreased mineralization of the upper part of the spine (Fig. 1C).

Altogether, the skeletal abnormalities of the ribs, limbs and vertebrae, and the lower mineral content observed were highly suggestive of altered ossification in LPA$_1^{(-/-)}$ mice.

LPA$_1^{(-/-)}$ mice display decreased vertebral and femoral trabecular bone

The bone phenotype of LPA$_1^{(-/-)}$ mice was further characterized by μCT analysis at 4 weeks of age. The findings of examination of vertebral and femoral microarchitecture are illustrated in Fig. 2. Measurements demonstrated a dramatically decreased bone volume over total volume (BV/TV) value in the trabecular bone of the vertebrae and femurs (81%, $p = 0.008$ and 77%, $p = 0.009$, respectively) (Figs. 2A, B, and C). This was essentially due to a reduction in trabecular number and thickness. Decreased connectivity and increased trabecular spacing were also observed (Fig. 2C). Similar changes were observed in the proximal femurs of LPA$_1^{(-/-)}$ mice, with a 62% reduction of BV/TV ($p = 0.05$) and a 58% decrease in trabecular number ($p = 0.05$) (Fig. 2C). SMI was higher in LPA$_1^{(-/-)}$ mice, indicative of a rod-like structure. Altogether, these results demonstrated significantly decreased bone mass in the vertebral and femoral trabecular bone of LPA$_1^{(-/-)}$ mice. Alizarin red

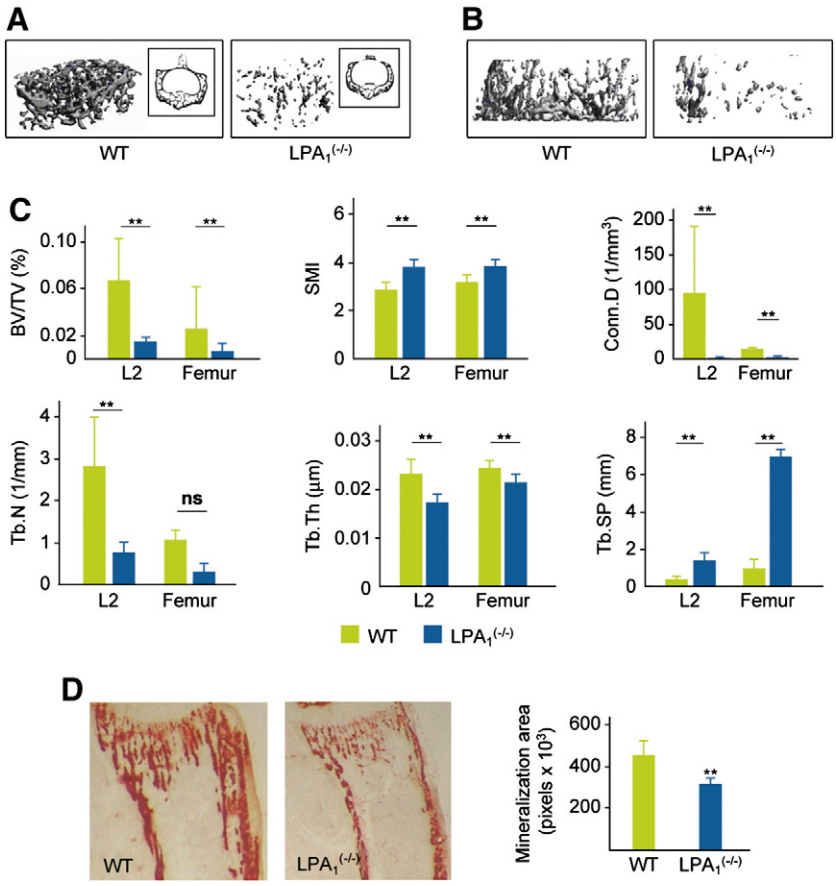

Fig. 2. Altered vertebral and femoral trabecular bone of $LPA_1^{(-/-)}$ mice. (A) µCT visualization of L_2 vertebra in 4-week-old $LPA_1^{(-/-)}$ mice and WT littermates (n = 6). (B) µCT visualization of trabecular area of the femur in 4-week-old $LPA_1^{(-/-)}$ mice and WT littermates (n = 6). (C) High resolution µCT parameters were measured in $LPA_1^{-/-}$ and WT mice (n = 6). Values analyzed in L_2 vertebrae and the trabecular area of the femur were BV/TV, bone volume/total volume; Tb.Th, trabecular thickness; Tb.N, trabecular number; Tb.Sp, trabecular spacing; Conn.D, connectivity density; SMI, structure model index. (D) Alizarin red (AR) staining of the proximal extremity of the tibia in 2-week-old $LPA_1^{(-/-)}$ mice and WT littermates. Mineralization area was quantified in pixels, $LPA_1^{(-/-)}$ (blue columns) and WT (green columns) (n = 4). Values are means (SD). Significant statistical differences between groups: *p < 0.05, **p < 0.01 for $LPA_1^{(-/-)}$ *vs.* WT by the Mann–Whitney test.

quantification of mineralized tissue in the proximal tibia also demonstrated a 30% decrease in $LPA_1^{(-/-)}$ mice (n = 6, $p < 0.002$) (Fig. 2D).

The cortical bone of $LPA_1^{(-/-)}$ mice also showed a 32% reduction in thickness (Figs. 3A and B). Cortical area (Ct.Ar) was significantly decreased by 37%, with marrow area (Ma.Ar) remaining unchanged (Fig. 3B).

The overall result of µCT studies demonstrated decreased bone mass in $LPA_1^{(-/-)}$ mice in both trabecular and cortical bone.

Material bone mineral density is not altered in $LPA_1^{(-/-)}$ mice

Altered bone density as observed by X-ray analysis may be variably due to defective mineralization (osteomalacia) and/or decreased bone mass (osteoporosis). The degree of mineralization of a given volume of bone (material density)[31] can, in first approach, be appreciated by µCT analysis. As shown in Fig. 4B, the material bone mineral density measured by µCT was not modified in the femoral cortex and vertebral trabecular bone of $LPA_1^{(-/-)}$ mice.

In order to confirm this result, we measured the mineral content of $LPA_1^{(-/-)}$ mice by infrared spectroscopy (Figs. 4C and D). Comparison of the relative intensities of the vibration bands produced by the collagenous phase with those of the mineral phase showed that mineralization of the cortical bone was similar in $LPA_1^{(-/-)}$ and WT mice (Fig. 4D). These observations were in agreement with the µCT data, suggesting decreased bone content (osteoporosis) with unchanged mineralization in $LPA_1^{(-/-)}$ mice. These data precluded

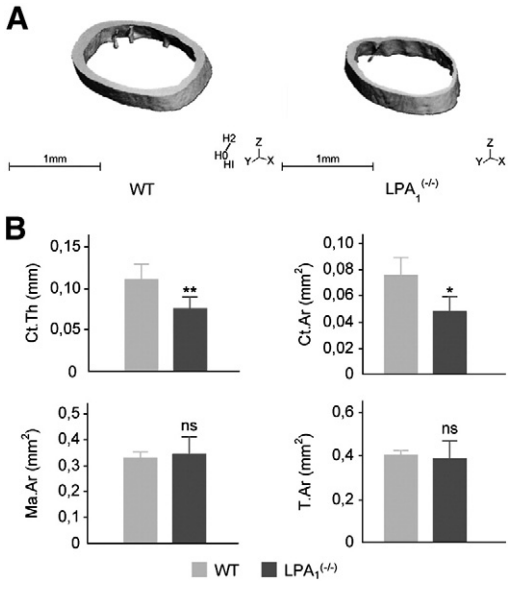

Fig. 3. Altered femoral cortical bone of $LPA_1^{(-/-)}$ mice. (A) µCT visualization of the cortical region of the femur in 4-week-old $LPA_1^{(-/-)}$ mice and WT littermates (n = 6). (B) High resolution µCT parameters were measured in femurs of six 4-week-old $LPA_1^{-/-}$ and WT mice as described in Materials and methods. Values analyzed were Ct.Th, cortical thickness; Ct.Ar, cortical area; Ma.Ar, marrow area; T.Ar, cross-sectional total area.Values are means (SD). Significant statistical differences between groups: *p < 0.05, **p < 0.001 for $LPA_1^{(-/-)}$ *vs.* WT by the Mann–Whitney test.

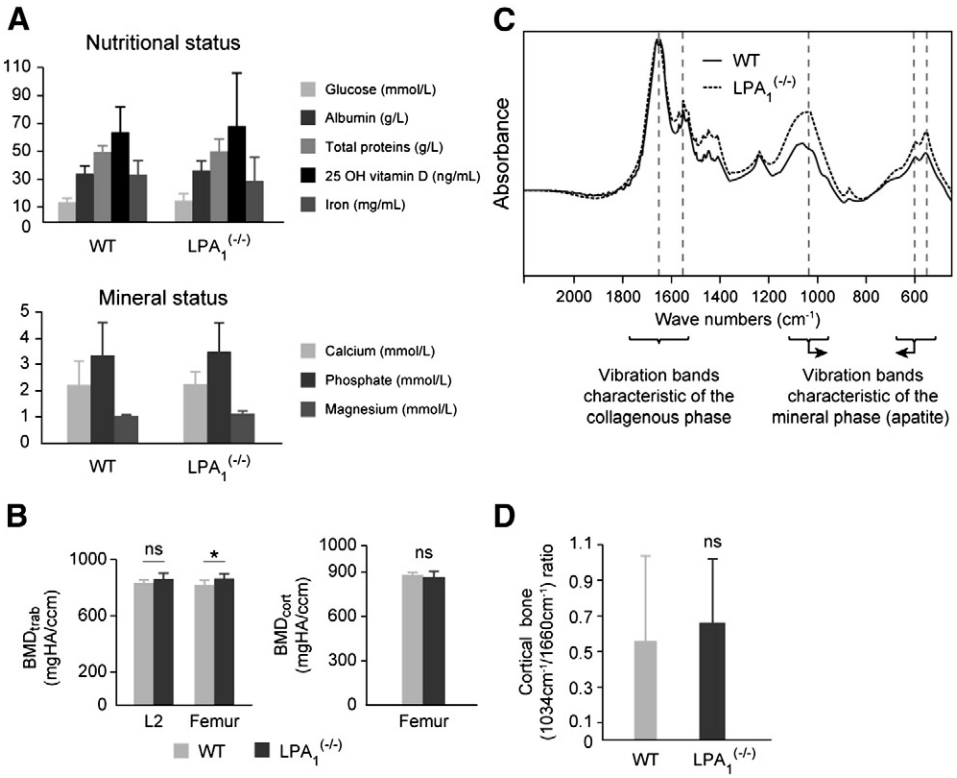

Fig. 4. Bone mineral density and mineral and nutritional status in LPA$_1^{(-/-)}$ mice. (A) μCT mineral density is conserved in LPA$_1^{(-/-)}$ mice.High resolution μCT parameters were measured in LPA$_1^{-/-}$ and WT mice (n = 6). Vertebral and femoral trabecular bone mineral density, BMD$_{trab}$, and femoral cortical bone mineral density, BMD$_{cort}$, were analyzed. (B) Nutritional and mineral status of LPA$_1^{(-/-)}$ mice.Values of serum glucose (mmol/l), albumin and total proteins (g/l), 25 OH vitamin D (ng/ml), iron (mg/l). These values were similar in the LPA$_1^{(-/-)}$ mice and WT littermates (n = 10). Values of total calcium, phosphate, and magnesium (mmol/l). Values were similar in the LPA$_1^{(-/-)}$ mice and WT littermates (n = 10). (C) Infrared spectra of the cortical area of femurs and tibiae did not show any clear difference between 4-week-old LPA$_1^{(-/-)}$ (dotted line) and WT mice (black line) (n = 8). (D) Ratio of the absorbance at 1034 and 1660 cm^{-1}, which reflects mineralization status (ratio of the mineral to organic phases) showed no differences between LPA$_1^{(-/-)}$ and WT mice (n = 8).Values are means (SD). Significant statistical differences between groups: *p<0.05, **p<0.001 of LPA$_1^{(-/-)}$ *vs.* WT mice by the Mann–Whitney test.

the hypothesis that osteomalacia alone could be responsible for the alteration of the bone tissue of LPA$_1^{(-/-)}$ mice.

Since decreased bone mass and/or mineralization may be secondary to alteration of nutritional status as well as calcium, phosphate, and vitamin D intake, we also investigated nutritional and mineral parameters in 4-week-old LPA$_1^{(-/-)}$ mice. Glucose, albumin, iron, and total protein plasma levels were similar in LPA$_1^{(-/-)}$ and WT mice, suggesting that the overall nutritional status of the surviving mice was not different from their WT littermates (Fig. 4A, upper). Moreover, no differences between LPA$_1^{(-/-)}$ and WT mice were observed (Fig. 4B, lower), ruling out disturbance of mineral homeostasis as a factor responsible for alteration of the skeletal phenotype.

Expression of osteoblast differentiation markers is decreased in LPA$_1^{(-/-)}$ mice

In order to better evaluate the impact of LPA$_1$ receptor deletion on the transcription of osteoblastic differentiation genes, the RNA levels of several bone markers were quantified by RT-PCR in the radius and femur (Fig. 5A). Most of the bone formation markers analyzed were decreased. The early indicator of osteoblast differentiation, collagen 1, was significantly decreased by 28% ($p = 0.04$). Osteocalcin levels were also significantly decreased by 35% ($p = 0.02$). Other markers of osteoblast differentiation, *i.e.* osterix, PTHR1 and DMP1, were also decreased in the bone of LPA$_1^{(-/-)}$ mice, by 20%, 22% and 30%, respectively, but this did not reach significance (Fig. 5A). Interestingly, the mRNA level of RUNX2 (runt-related transcription factor 2), a transcription factor required for initial mesenchymal stem cell differentiation toward the osteoblastic lineage and acting upstream of osterix, was unchanged in LPA$_1^{(-/-)}$ mice compared with their WT littermates (data not shown).

Taken together, these data demonstrate that some markers of osteoblastic differentiation, collagen 1 and osteocalcin, are significantly less expressed in LPA$_1^{(-/-)}$ mouse bones. All markers demonstrated a tendency to decrease, suggesting that the overall osteoblastic differentiation process is altered in LPA$_1^{(-/-)}$ mice.

In order to document the level of remodeling, we also investigated the expression of RANK, RANKL and OPG in WT and LPA$_1^{(-/-)}$ mouse bones. The mRNA level of these genes was similar in LPA$_1^{(-/-)}$ mice and WT littermates (Fig. 5B), indicating that osteoclasis, at least in long bones at this stage of development, is unaffected by the loss of the LPA$_1$ receptor and is therefore not responsible for the altered bone mass. In keeping with these observations, the serum level of CTX-I, a marker of collagen 1 degradation, was unchanged in LPA$_1^{(-/-)}$ mice compared with WT littermates (Fig. 5C).

Other LPA receptors, especially LPA$_4$, may influence bone differentiation and bone mass [20]. Expression of LPA receptors was therefore also evaluated by RT-PCR in femurs and tibias of LPA$_1^{(-/-)}$ mice. Expression of autotaxin (ATX), a major enzyme involved in LPA production, was also quantified. Expression of LPA$_2$ LPA$_3$ and LPA$_4$ and ATX was similar in LPA$_1^{(-/-)}$ mice and WT littermates (Fig. 5D). As a control, Fig. 5E demonstrates that, as expected, LPA$_1$ is expressed in bones of WT mice but not in the LPA LPA$_1^{(-/-)}$ strain. LPA concentration in plasma did not differ between LPA$_1^{(-/-)}$ mice and WT littermates (209 (±67) *vs* 189 (±70) pmol/ml, n = 4, NS, in LPA$_1^{(-/-)}$ mice and WT littermates respectively (Fig. 5F).

Absence of LPA$_1$ therefore seems specifically to influence *in vivo* bone formation, with no significant effect on bone resorption. In addition, the bone phenotype of LPA$_1^{(-/-)}$ mice does not seem due to a modified expression of other LPA receptors or a variation of LPA production.

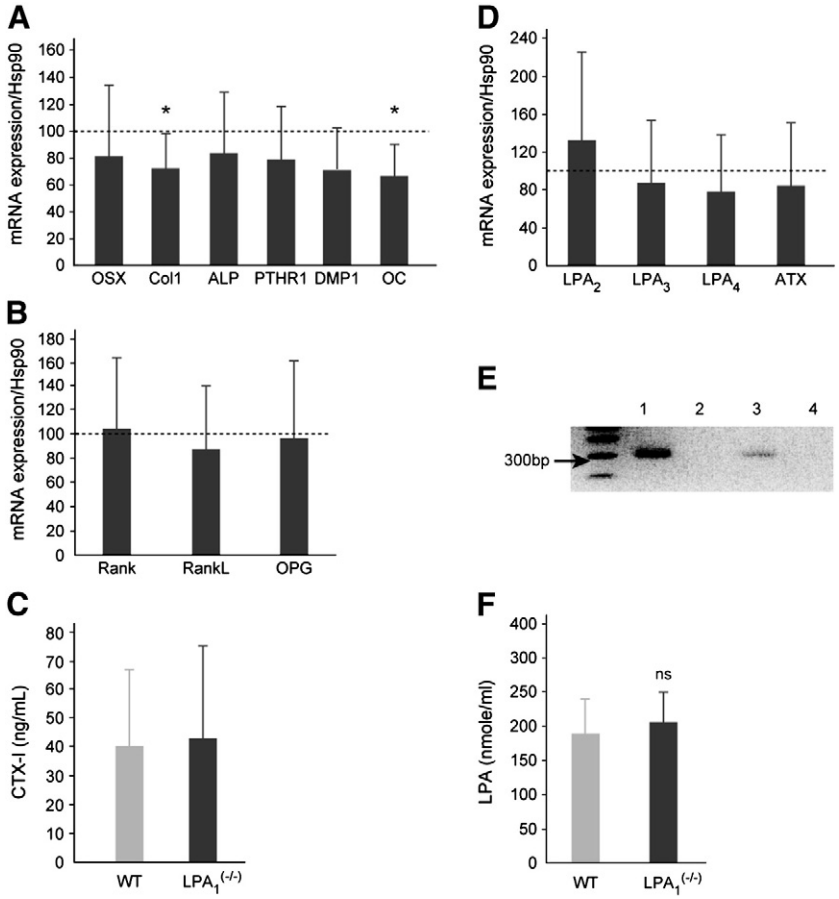

Fig. 5. Expression of bone markers and LPA receptors in LPA$_1^{(-/-)}$ mice. (A) Real time RT-PCR of bone markers in long bones of LPA$_1^{(-/-)}$ mice: RNAs were extracted from the humerus and radius of 4-week-old LPA$_1^{(-/-)}$ mice and WT littermates (n = 9). Expression of collagen 1a (Col 1), alkaline phosphatase (ALP), osterix (OST), osteocalcin (OC), PTH receptor 1 (PTHR1) and dentin matrix protein 1 (DMP1) was tested. Dashed line represents the level normalized to 100% of values observed in WT mice. Columns represent the level of gene expression in LPA$_1^{(-/-)}$ mice. (B) Expression of receptor activator of nuclear factor κB (RANK), receptor activator of nuclear factor κB-ligand (RANKL) and osteoprotegerin (OPG) was tested. Dashed line represents the level normalized to 100% of values observed in WT mice. Columns represent the level of gene expression in LPA$_1^{(-/-)}$ mice. (C) Values of serum CTX-I (ng/mL), reflecting collagen I degradation, were similar in LPA$_1^{(-/-)}$ mice and WT littermates (n = 7). (D) Expression of LPA$_2$, LPA$_3$, LPA$_4$ and autotaxin (ATX) was assessed by real time RT-PCR. Dashed line represents the level normalized to 100% of values observed in the WT. Columns represent the level of gene expression in LPA$_1^{(-/-)}$ mice. (E) PCR detection of LPA$_1$ receptor in WT and LPA$_1^{(-/-)}$ mice. Lanes 1 and 2 represent the genomic detection by PCR of LPA$_1$ receptor in DNA of WT and LPA$_1^{(-/-)}$ mice, respectively. Lanes 3 and 4 represent the detection by RT-PCR of LPA$_1$ receptor in bones of WT mice of LPA$_1^{(-/-)}$ mice respectively.(F) LPA concentration in plasma from LPA$_1^{(-/-)}$ and WT mice. LPA concentration was evaluated in fasting mice as described in Materials and methods. Values are not significantly different between LPA$_1^{(-/-)}$ and WT mice. Values are means (SD). Significant statistical differences between groups: *$p < 0.05$ of LPA$_1^{(-/-)}$ *vs.* WT by the Mann–Whitney test.

LPA$_1^{(-/-)}$ mBMSC exhibit impaired proliferation and differentiation processes in vitro

To further investigate whether the impaired bone formation is the result of defective osteoblast proliferation and differentiation, we cultured murine bone marrow mesenchymal stem cells (mBMSC) from LPA$_1^{(-/-)}$ and WT mice. The proliferation rate of mBMSC was tested in basal medium with 10% FCS for 3, 7 and 10 days (Fig. 6A). After decreasing at D3, the DNA content of WT mBMSC increased significantly at D7 and D10. The DNA content was dramatically decreased in LPA$_1^{(-/-)}$ mBMSC (Fig. 6A).

The osteoblastic differentiation of WT and LPA$_1^{(-/-)}$ mBMSC was also tested in osteogenic medium. Alizarin red S staining showed highly decreased mineralization in LPA$_1^{(-/-)}$ cultured mBMSC (Fig. 6B).

Discussion

Several *in vitro* studies have so far demonstrated that LPA is involved both in osteoblastic differentiation [10–12,14,15,18,19] and in osteoclast activity [13]. LPA interacts with a set of G-protein-coupled receptors, such as LPA$_1$ and LPA$_4$, which are expressed in bone cells. While LPA$_4$, likely associated to increase of cAMP [9], inhibits osteogenic differentiation [20], so far available *in vitro* data strongly suggests that LPA$_1$ has a possible role in promoting bone formation. The current model in fact supports the hypothesis of LPA production by osteoblasts, possibly promoting both osteoblastic differentiation and osteoclasis [13]. Therefore, the absence of LPA$_1$ may theoretically contribute to either increase or decrease the overall bone mass. The results presented here demonstrate that LPA$_1^{(-/-)}$ mice display bone abnormalities and osteoporosis, suggesting a prominent role of LPA$_1$ in osteogenesis.

The bone developmental abnormalities observed in LPA$_1^{(-/-)}$ mice affected the ribs and vertebrae. Attachment of the ribs to the sternum was abnormal, with fusion of the ribs observed in all LPA$_1^{(-/-)}$ mice. Fused ribs are observed in a variety of conditions, for example disruption of the transcription factor Hoxa-9 which results in fusion of the first and second ribs [32,33], and more recent data have described multiple developmental factors involved in rib formation. In particular, *Hand2* overexpression resumes some of the abnormalities observed in LPA$_1$ mice [34]. Nevertheless, absence of the bone morphogenetic proteins BMP-4 and BMP-7 is also responsible for abnormal costo-sternal connections [35]. There is to our knowledge no published data

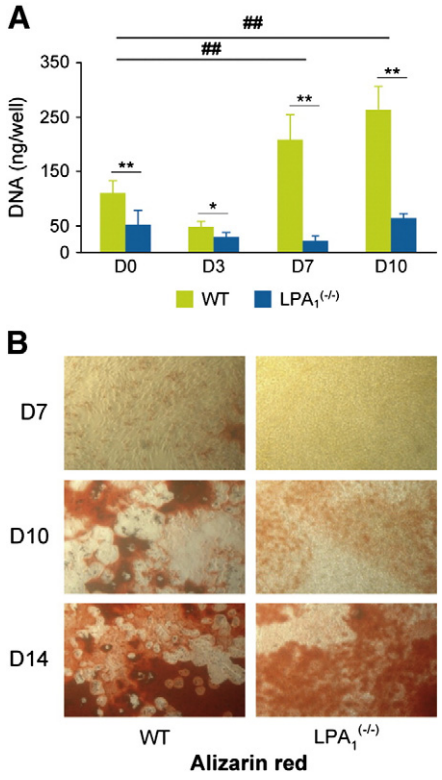

Fig. 6. $LPA_1^{(-/-)}$ mBMSC display decreased proliferation and mineralization. (A) WT and $LPA_1^{(-/-)}$ mBMSC were seeded and cultured for 2 days (D0) in medium with 10% FCS (see Materials and methods) and tested at D0, D3, D7 and D10, and DNA content was measured using the Picogreen® assay. (B) mBMSC were cultured in osteogenic medium for 7, 10, or 14 days and stained with alizarin red S solution to evaluate mineralization. Lower mineralization at D7 and D10 was observed in $LPA_1^{(-/-)}$ mBMSC cultures. Values are means (SD). Significant statistical differences between groups: ##$p<0.001$ of WT D0 *vs.* D7 or D10; *$p<0.05$, **$p<0.001$ of $LPA_1^{(-/-)}$ *vs.* WT by the Mann–Whitney test.

indicating that LPA_1 interferes with such processes and, so far, no identified disease clearly resumes the abnormalities observed in $LPA_1^{(-/-)}$ mice.

$LPA_1^{(-/-)}$ mice also demonstrated low trabecular and cortical bone mass. These mice had low trabecular bone volume and decreased trabecular number and thickness, both vertebral and femoral trabecular bones being affected. The altered SMI was also indicative of a potentially fragile network. Femoral cortical thickness was also significantly decreased in $LPA_1^{(-/-)}$ mice. They were therefore severely affected by a global bone defect, suggestive of osteoporosis. Notably, $LPA_1^{(+/-)}$ animals were fully exempt from any abnormal bone phenotype, and no significant differences between male and females were observed. Indeed, the growth phenotype, affecting vertebrae and limbs, is suggestive of abnormal endochondral ossification. However cortical thickness was also decreased, suggesting an overall alteration of osteogenesis in the absence of LPA_1. In accordance with this finding, the decreased expression of early and late markers of osteoblastic differentiation suggests that LPA_1 is significantly involved in bone formation.

The findings obtained with cultured mBMSC are consistent with the data observed *in vivo*. The $LPA_1^{(-/-)}$ mBMSC demonstrated a highly decreased proliferation rate, in keeping with the effect of $LPA_1^{(-/-)}$ as a growth factor in osteoblastic models [11,12]. The decreased mineralization of $LPA_1^{(-/-)}$ mBMSC suggests that their decreased proliferation also impairs their further mineralization. These results, which show the specific impact of the absence of LPA_1 in bone progenitors, are consistent with previous reports obtained in osteoblastic cell lines [14,18,19,36].

Interestingly, as demonstrated by μCT and infrared analysis, the bone mineral deficiency observed in $LPA_1^{(-/-)}$ mice seems related to true osteoporosis without a mineralization deficiency as such. The mineral density measured by μCT in both trabecular and cortical bone was not significantly decreased in $LPA_1^{(-/-)}$ mice. The ratio of mineralized to organic phase measured by infrared analysis, as a reflect of the material bone mineral density, was even slightly higher in the bones of $LPA_1^{(-/-)}$ mice, which may be indicative of a compensatory mechanism to osteoporosis or alteration of mineralization kinetics as observed in *osteogenesis imperfecta* [37,38]. In parallel, the major parameters involved in the overall control of bone mass, including calcium, phosphate, and vitamin D, were not modified in $LPA_1^{(-/-)}$ mice, nor were nutrition parameters.

Of particular interest is the surprising interplay of the different LPA receptors that are thought to act during osteogenesis and are potentially involved in the regulation of bone mass. Recent studies and our data suggest that LPA_1 and LPA_4 receptors display completely opposite effects on the development of bone mass, with LPA_4 exerting a negative effect [20] and LPA_1 a positive one. LPA_1 has been described as activating several intracellular cascades, namely G_i, G_q and $G_{12/13}$ pathways [6]. The G_i pathway is usually associated with an increased proliferation rate and seems involved in osteoblastic proliferation under LPA [11,12]. Nevertheless, overexpression of the G_i pathway has also been recently associated with decreased osteogenesis [39]. Therefore, it can be hypothesized that LPA_1 participation in tuning of the G_i pathway is necessary to optimize osteoblastic proliferation and differentiation and eventually osteogenesis.

The effect of LPA_1 on bone resorption has been documented in the bone metastasis process [40], and a role of the LPA_1/Gi pathway in osteoclast activation has recently been demonstrated [13]. Here, the overall effect *in vivo* of LPA_1 was to decrease bone mass and, supposedly, to lower the osteogenesis rate.

Indeed, the potential effect of LPA on osteogenesis or osteoclasis may depend on the respective expression of LPA receptors by bone cells and the concentration of LPA in the tissue. In this view, the potency of specific molecular species of LPA towards LPA_1 and LPA_4 is variable [9]. In parallel, distinct mechanisms may be involved in the control of the paracrine secretion of LPA [3–5], several data supporting the hypothesis of LPA production in bone tissue itself [19,40]. Osteoblasts secrete LPA through activation of phospholipase C and phospholipase A_2 pathways [19]. We also observed that human MSC also produce significant levels of secreted LPA (personal unpublished results). In addition, platelets may contribute to significant increase of the local concentration of LPA in bone tissues [5,40]. In this view, we found no indication in our study of a modification of either the level of circulating LPA or the expression of autaxin, the main enzyme involved in LPA production, in $LPA_1^{(-/-)}$ mice. In parallel, the expression of other LPA receptors was not modified in the bone tissue of $LPA_1^{(-/-)}$ mice, suggesting that their bone phenotype, and osteoporosis in particular, can be attributed to the absence of LPA_1 alone.

Conclusion

In summary, the results of our study help to clarify the role of LPA_1 *in vivo*. $LPA_1^{(-/-)}$ mice display defects in bone formation with osteoporosis as consequence, as well as specific developmental abnormalities, indicating that the LPA_1 receptor is significantly involved in osteogenesis. Notably, the active emergence of therapeutics involving lysophospholipids and their receptors could include bone as a future target of LPA receptor modulation.

Acknowledgments

We thank N. Laroche, of INSERM U890 and Saint-Etienne University, for technical assistance in μCT analysis. We thank E. Gouze of INSERM UMR 1043 for critical discussion. We also thank A. Tridon of the animal research facility and C. Carriven, A. Bros, M. Nieto and L. Micheletti for their technical support. We thank J.S. Saulnier-Blache for providing us with recombinant rat LPA acyl-transferase.

References

[1] Ralston SH, Uitterlinden AG. Genetics of osteoporosis. Endocr Rev 2010;31: 629–62.
[2] Chun J, Hla T, Lynch KR, Spiegel S, Moolenaar WH. International Union of Basic and Clinical Pharmacology. LXXVIII. Lysophospholipid receptor nomenclature. Pharmacol Rev 2010;62:579–87.
[3] Fourcade O, Simon MF, Viode C, Rugani N, Leballe F, Ragab A, et al. Secretory phospholipase A2 generates the novel lipid mediator lysophosphatidic acid in membrane microvesicles shed from activated cells. Cell 1995;80:919–27.
[4] Gaits F, Fourcade O, Le Balle F, Gueguen G, Gaige B, Gassama-Diagne A, et al. Lysophosphatidic acid as a phospholipid mediator: pathways of synthesis. FEBS Lett 1997;410:54–8.
[5] Ferry G, Tellier E, Try A, Gres S, Naime I, Simon MF, et al. Autotaxin is released from adipocytes, catalyzes lysophosphatidic acid synthesis, and activates preadipocyte proliferation. Up-regulated expression with adipocyte differentiation and obesity. J Biol Chem 2003;278:18162–9.
[6] Noguchi K, Herr D, Mutoh T, Chun J. Lysophosphatidic acid (LPA) and its receptors. Curr Opin Pharmacol 2009;9:15–23.
[7] Choi J, Herr D, Noguchi K, Yung Y, Lee C, Mutoh T, et al. LPA receptors: subtypes and biological actions. Annu Rev Pharmacol Toxicol 2010;50:157–86.
[8] Lin ME, Herr DR, Chun J. Lysophosphatidic acid (LPA) receptors: signaling properties and disease relevance. Prostaglandins Other Lipid Mediat 2010;91:130–8.
[9] Tigyi G. Aiming drug discovery at lysophosphatidic acid targets. Br J Pharmacol 2010;161:241–70.
[10] Caverzasio J, Palmer G, Suzuki A, Bonjour JP. Evidence for the involvement of two pathways in activation of extracellular signal-regulated kinase (Erk) and cell proliferation by Gi and Gq protein-coupled receptors in osteoblast-like cells. J Bone Miner Res 2000;15:1697–706.
[11] Grey A, Banovic T, Naot D, Hill B, Callon K, Reid I, et al. Lysophosphatidic acid is an osteoblast mitogen whose proliferative actions involve G(i) proteins and protein kinase C, but not P42/44 mitogen-activated protein kinases. Endocrinology 2001;142:1098–106.
[12] Ahmed I, Gesty-Palmer D, Drezner MK, Luttrell LM. Transactivation of the epidermal growth factor receptor mediates parathyroid hormone and prostaglandin F2 alpha-stimulated mitogen-activated protein kinase activation in cultured transgenic murine osteoblasts. Mol Endocrinol 2003;17:1607–21.
[13] Lapierre DM, Tanabe N, Pereverzev A, Spencer M, Shugg RPP, Dixon SJ, et al. Lysophosphatidic acid signals through multiple receptors in osteoclasts to elevate cytosolic calcium concentration, evoke retraction, and promote cell survival. J Biol Chem 2010;285:25792–801.
[14] Gidley J, Openshaw S, Pring ET, Sale S, Mansell JP. Lysophosphatidic acid cooperates with 1alpha,25(OH)2D3 in stimulating human MG63 osteoblast maturation. Prostaglandins Other Lipid Mediat 2006;80:46–61.
[15] Karagiosis SA, Karin NJ. Lysophosphatidic acid induces osteocyte dendrite outgrowth. Biochem Biophys Res Commun 2007;357:194–9.
[16] Waters KM, Jacobs JM, Gritsenko MA, Karin NJ. Regulation of gene expression and subcellular protein distribution in MLO-Y4 osteocytic cells by lysophosphatidic acid: relevance to dendrite outgrowth. Bone 2011;48:1328–35.
[17] Masiello LM, Fotos JS, Galileo DS, Karin NJ. Lysophosphatidic acid induces chemotaxis in MC3T3-E1 osteoblastic cells. Bone 2006;39:72–82.
[18] Panupinthu N, Zhao L, Possmayer F, Ke HZ, Sims SM, Dixon SJ. P2X7 nucleotide receptors mediate blebbing in osteoblasts through a pathway involving lysophosphatidic acid. J Biol Chem 2007;282:3403–12.
[19] Panupinthu N, Rogers JT, Zhao L, Solano-Flores LP, Possmayer F, Sims SM, et al. P2X7 receptors on osteoblasts couple to production of lysophosphatidic acid: a signaling axis promoting osteogenesis. J Cell Biol 2008;181:859–71.
[20] Liu YB, Kharode Y, Bodine PV, Yaworsky PJ, Robinson JA, Billiard J. LPA induces osteoblast differentiation through interplay of two receptors: LPA1 and LPA4. J Cell Biochem 2010;109:794–800.
[21] Contos JJ, Fukushima N, Weiner JA, Kaushal D, Chun J. Requirement for the lpA1 lysophosphatidic acid receptor gene in normal suckling behavior. Proc Natl Acad Sci U S A 2000;97:13384–9.
[22] Dingerkus G, Uhler LD. Enzyme clearing of alcian blue stained whole small vertebrates for demonstration of cartilage. Stain Technol 1977;52:229–32.
[23] Kohlbrenner A, Koller B, Hammerle S, Ruegsegger P. In vivo micro tomography. Adv Exp Med Biol 2001;496:213–24.
[24] David V, Laroche N, Boudignon B, Lafage-Proust MH, Alexandre C, Ruegsegger P, et al. Noninvasive in vivo monitoring of bone architecture alterations in hindlimb-unloaded female rats using novel three-dimensional microcomputed tomography. J Bone Miner Res 2003;18:1622–31.
[25] Oreffo RO, Kusec V, Romberg S, Triffitt JT. Human bone marrow osteoprogenitors express estrogen receptor-alpha and bone morphogenetic proteins 2 and 4 mRNA during osteoblastic differentiation. J Cell Biochem 1999;75:382–92.
[26] Stanford CM, Jacobson PA, Eanes DE, Lembke LA, Midura RJ. Rapidly forming apatitic mineral in osteoblastic cell line (UMR 10601 BSP). J Biol Chem 1995;270: 9420–8.
[27] Thèves C, Keyser-Tracqui C, Crubézy E, Salles JP, Ludes B, Telmon N. Detection and quantification of the age-related point mutation A189G in the human mitochondrial DNA. Forensic Sci 2006;51:865–73.
[28] Saulnier-Blache JS, Girard A, Simon MF, Lafontan M, Valet P. A simple and highly sensitive radioenzymatic assay for lysophosphatidic acid quantification. J Lipid Res 2000;41:1947–51.
[29] Chang MC, Tanaka J. FT-IR study for hydroxyapatite/collagen nanocomposite cross-linked by glutaraldehyde. Biomaterials 2002;23:4811–8.
[30] Boskey AL, Goldberg M, Ashok K, Santiago G. Infrared imaging microscopy of bone: illustrations from a mouse model of Fabry disease. Biochim Biophys Acta 2006;1758:942–7.
[31] Rauch F, Schoenau E. Changes in bone density during childhood and adolescence: an approach based on bone's biological organization. J Bone Miner Res 2001;16:597–604.
[32] Chen F, Capecchi MR. Targeted mutations in hoxa-9 and hoxb-9 reveal synergistic interactions. Dev Biol 1997;181:186–96.
[33] McIntyre DC, Rakshit S, Yallowitz AR, Loken L, Jeannotte L, Capecchi MR, et al. Hox patterning of the vertebrate rib cage. Development 2007;134:2981–9.
[34] Abe M, Michikami I, Fukushi T, Abe A, Maeda Y, Ooshima T, et al. Hand2 regulates chondrogenesis in vitro and in vivo. Bone 2010;46:1359–68.
[35] Katagiri T, Boorla S, Frendo JL, Hogan BL, Karsenty G. Skeletal abnormalities in doubly heterozygous Bmp4 and Bmp7 mice. Dev Genet 1998;22:340–8.
[36] Grey A, Xu X, Hill B, Watson M, Callon K, Reid IR, et al. Osteoblastic cells express phospholipid receptors and phosphatases and proliferate in response to sphingosine-1-phosphate. Calcif Tissue Int 2004;74:542–50.
[37] Fratzl P, Paris O, Klaushofer K, Landis WJ. Bone mineralization in an osteogenesis imperfecta mouse model studied by small-angle x-ray scattering. J Clin Invest 1996;97:396–402.
[38] Roschger P, Fratzl-Zelman N, Misof BM, Glorieux FH, Klaushofer K, Rauch F. Evidence that abnormal high bone mineralization in growing children with osteogenesis imperfecta is not associated with specific collagen mutations. Calcif Tissue Int 2008;82:263–70.
[39] Yadav VK, Ryu JH, Suda N, Tanaka KF, Gingrich JA, Schutz G, et al. Lrp5 controls bone formation by inhibiting serotonin synthesis in the duodenum. Cell 2008;135: 825–37.
[40] Boucharaba A, Serre CM, Gres S, Saulnier-Blache JS, Bordet JC, Guglielmi J, et al. Platelet-derived lysophosphatidic acid supports the progression of osteolytic bone metastases in breast cancer. J Clin Invest 2004;114:1714–25.